HHS Public Access

Author manuscript

Cancer Lett. Author manuscript; available in PMC 2019 October 01.

Published in final edited form as:

Cancer Lett. 2018 October 01; 433: 1–9. doi:10.1016/j.canlet.2018.06.025.

High collagen density augments mTOR-dependent cancer stem cells in ERα+ mammary carcinomas, and increases mTOR-independent lung metastases

Michael P. Shea[a,b], **Kathleen A. O'Leary**[b], **Kyle A. Wegner**[a,b], **Chad M. Vezina**[a,b,c], and **Linda A. Schuler**[a,b,c]

[a]Molecular and Environmental Toxicology Program, University of Wisconsin-Madison, Madison, WI, USA

[b]Department of Comparative Biosciences, University of Wisconsin-Madison, Madison, WI, USA

[c]University of Wisconsin Paul P. Carbone Comprehensive Cancer Center, University of Wisconsin-Madison, WI, USA

Abstract

Metastatic estrogen receptor alpha positive (ERα+) cancers account for most breast cancer mortality. Cancer stem cells (CSCs) and dense/stiff extracellular matrices are implicated in aggression and therapy resistance. We examined this interplay and response to mTOR inhibition using ERα+ adenocarcinomas from NRL-PRL females in combination with *Col1a1*$^{tmJae/+}$ (mCol1a1) mice, which accumulate collagen-I around growing tumors. Orthotopic transplantation of tumor cells to mCol1a1 but not wildtype hosts resulted in striking desmoplasia. Mammary tumors in mCol1a1 recipients displayed higher CSC activity and enhanced AKT-mTOR and YAP activation, and these animals developed more and larger lung metastases. Treatment with the mTOR inhibitor, rapamycin, with or without the anti-estrogen, ICI182780, rapidly diminished mammary tumors, which rapidly reversed when treatment ceased. In contrast, lung metastases, which exhibited lower proliferation and pS6RP, indicating lower mTOR activity, were unresponsive, and mCol1a1 hosts continued to sustain greater metastatic burdens. These findings shed light on the influence of desmoplastic tumor microenvironments on the CSC niche and metastatic behavior in ERα+ breast cancer. The differential mTOR dependence of local mammary tumors and pulmonary lesions has implications for success of mTOR inhibitors in advanced ERα+ disease.

Corresponding author: Linda A. Schuler, University of Wisconsin-Madison, 2015 Linden Dr., Madison, WI 53706. Phone: 608-263-9825; Fax: 608-263-3926. linda.schuler@wisc.edu.

Conflict of Interest

The authors declare no potential conflicts of interest.

Keywords

breast cancer; luminal B subtype; extracellular matrix density/stiffness; cancer stem cells; mTOR

1. Introduction

Patients with estrogen receptor alpha (ERα) expressing tumors constitute 75% of breast cancer cases. Though often treated successfully with surgery and anti-estrogen therapies, approximately 25% initially or eventually display treatment resistance and recurrence of metastatic disease [1, 2]. Unfortunately, little is known about the mechanisms which contribute to progression and therapeutic insensitivity of these cancers, but increasing evidence implicates components of the tumor microenvironment, such as the extracellular matrix (ECM), as partners in these processes.

Collagen density, organization and tissue stiffness have been independently linked to mammary cancer. Type-1 fibrillar collagens are prevalent in the mammary ECM, and dense collagen is associated with increased risk of breast cancer [3]. Collagen organization, particularly alignment of collagen fibers perpendicular to the tumor boundary, correlates with reduced survival of patients with ERα+ cancers [4]. Furthermore, increased tissue stiffness, which can be conferred by accumulated collagen, contributes to tumor cell invasion and treatment resistance [5–7]. The mechanism(s) by which desmoplastic microenvironments drive tumor aggression is not fully understood, but may involve cancer cells with stem-like characteristics [8–10]. Cancer stem cells (CSCs) have the ability to regenerate tumor heterogeneity and self-renew [11, 12]. Signaling through the mammalian target of rapamycin (mTOR) increases activity of CSCs in breast cancers [13–15]. Inhibition of mTOR signaling by the rapamycin analog, everolimus, has been approved for treatment of patients with anti-estrogen resistant ERα+ breast cancer [16–18]. However, how desmoplastic environments affect responses of ERα+ cancers to these therapies is not known.

To investigate the links among collagen density/stiffness, CSCs, metastatic behavior, and treatment sensitivity of ERα+ breast cancer *in vivo*, we utilized the metastatic ERα+ mammary adenocarcinomas that develop in nulliparous transgenic NRL-PRL females [19]. These prolactin-induced serially transplantable, lineage heterogeneous ERα+ cancers [20] provide a preclinical model to investigate responses of complex cancers in immunocompetent environments. These tumors exhibit ER-responsive gene expression, but many lose dependence on ER-mediated signals for growth [20], modeling advanced anti-estrogen resistant clinical breast cancers. To evaluate the impact of desmoplastic tumor microenvironments, we employed a genetically engineered mouse with a mutation in the c*ol1a1* gene (c$ol1a1^{tm1Jae}$), rendering it non-cleavable [21]. In this model, the desmoplastic c$ol1a1^{tm1Jae/+}$ (mCol1a1) environment increases the multiplicity of primary tumors and metastases in MMTV-PyMT mice [22], and intravasation and lung metastases of orthotopically transplanted mammary tumor cell lines [23]. Here, we transplanted serially passaged ERα+ tumor cells into mammary fat-pads of either wildtype (WT) or mCol1a1 recipients. Mammary tumors in mCol1a1 recipients were surrounded by dense collagen

fibers which aligned more perpendicularly to tumor boundaries. These tumors exhibited higher CSC activity, driven by the AKT-mTOR signaling cascade and YAP, a major downstream effector of the Hippo signaling pathway. Further, mCol1a1 recipients developed more and larger lung metastases. Treatment of tumor-burdened mice with the mTOR inhibitor, rapamycin, with or without the selective estrogen downregulator (SERD), ICI 182,780 (ICI), dramatically reduced the size and CSC activity of mammary tumors in both recipient genotypes. However, in contrast to the rapamycin sensitivity of the local tumors, lung metastases did not respond to inhibition of mTOR signaling, and mCol1a1 hosts continued to sustain greater metastatic burdens. Closer examination revealed that metastases displayed lower mTOR activity and rates of proliferation than mammary tumors. This failure of lung metastases to respond to mTOR-targeted therapy underscores the need to understand and target processes which lead to treatment evasion, particularly at distant sites.

2. Materials and methods

2.1 Experimental mice and treatment administration

Animals were bred, handled, and housed in accordance with the National Institutes of Health Guide for Care and Use of Laboratory Animals in AAALAC-accredited facilities. All procedures were approved by the University of Wisconsin-Madison Institutional Animal Care and Use Committee. NRL-PRL mice were generated and maintained on the FVB/N strain background [24]. Heterozygous c*ol1a1*^{tm1Jae} (mCol1a1) mice [21] were backcrossed for more than 10 generations onto the FVB/N strain. A primary ERα+ NRL-PRL adenocarcinoma (#72-46) [20], which has been serially passaged *in vivo,* was digested into a single-cell suspension for subsequent transplantations into 8-week old wild-type (WT) and mCol1a1 syngeneic recipients. 100,000 cells were injected bilaterally into intact caudal mammary glands of recipient mice, and growth of tumors was monitored using digital calipers. Tumor volume was calculated as: largest diameter * (smallest diameter^2) * 0.4. When tumors reached 150 mm^3, mice were divided into treatment cohorts: untreated control, ICI 182,780 (ICI, Fulvestrant, AstraZeneca Pharmaceuticals, weekly subcutaneous injection, 250 mg/kg), Rapamycin (Rapamune oral solution, Pfizer Inc., daily oral gavage, 5 mg/kg), and ICI/Rapamycin combination therapy. The bioactivity of ICI *in vivo* was confirmed by reduced uterine weights (Fig. S1A). For some studies, animals were euthanized after 2 or 14 days of treatment. For an additional cohort (withdrawal, WD), mice that had been treated with ICI/Rapamycin for 14 days were untreated for an additional 14 days prior to tissue collection.

2.2 Immunohistochemistry

Portions of tumors were fixed overnight in 10% neutral buffered formalin, and processed into 5 μm sections for immunostaining [25]. Sections were counterstained with hematoxylin and imaged using an E600 Eclipse microscope with NIS-Elements imaging software. The following antibodies were used: ERα (1/500; Santa Cruz Biotechnology, #SC-542), pAKT^{S473} (1/50; Cell Signaling Technologies, #3787), YAP (1/400; Cell Signaling Technologies, #14074), cleaved caspase-3 (Asp175) (1/100; Cell Signaling Technologies, #9661), pp70S6K (1/100; Cell Signaling Technologies, #9205), Ki-67 (1:500; Abcam, #15580), pS6RP$^{S235/236}$ (1/400; Cell Signaling Technologies, #4858), and biotinylated anti-

rabbit IgG (H&L) (Vector Laboratories, #BA-1000). Labeled cells were quantified by counting 200 cells in each of five random 40x fields of view (FOV) for each tumor.

All lungs from tumor-burdened mice were processed as above, and metastatic load was quantified in three step-sections, 50 μm apart. Metastases in ten random 10x FOVs were counted in each section, taking care to avoid recounting metastases which spanned multiple step-sections. Lesion area was quantified by tracing freehand perimeters using ImageJ software [26].

2.3 Collagen fiber imaging and analysis

Fibrillar collagens were analyzed by staining sections with picrosirius red, and visualized at high resolution using fluorescent microscopy methodology [27]. Stained fibrillar collagens produce a robust fluorescent signal when excited using a 561 nm laser with emission detection between 635–685 nm, improving imaging quality over polarized light microscopy. Imaging was performed using a Leica TCS SP8 confocal microscope with LAS X software and a scanning tile-stitching 20x oil-immersion objective. Quantification of total collagen fiber number was performed utilizing CT-FIRE software (LOCI, Madison, WI), and alignment was analyzed using CurveAlign software (LOCI, Madison, WI) [28]. Collagen fibers in five random 20x FOVs for each tumor were analyzed.

2.4 Tumorsphere formation in vitro

Single-cell suspensions were prepared from harvested tumors as described [20] for subsequent analyses. In brief, fragments were dissociated in Epicult-B Mouse Medium (Stem Cell Technologies, #05610) supplemented with 5% fetal bovine serum, 10 ng/mL epidermal growth factor, 300 U/mL collagenase, and 100 U/mL hyaluronidase (Stem Cell Technologies, #07912) at 37°C for one hour. Red blood cells were lysed using ammonium chloride, and then cells were incubated for one minute in trypsin-EDTA (Stem Cell Technologies, #07901) containing 5 mg/mL dispase (Stem Cell Technologies, #07913) and 0.1 mg/mL DNase I (Stem Cell Technologies, #07900), and filtered through 40 μm strainers. Cancer stem cell activity was quantified using the *in vitro* mammosphere formation assay [29, 30] as described [20]. Briefly, single-cell suspensions of 4 independent tumors were seeded at six replicates of 25,000 cells/well into 96-well ultra-low attachment plates (Corning, #3474) in mammosphere medium containing DMEM-F12 with 20 ng/mL EGF, 20 ng/mL bFGF, 1X B27 supplement (Gibco, #17504044), 5 μg/mL insulin, and 100 μg/mL gentamicin. After 10 days of culture at 37°C, tumorspheres greater than 50 μm in diameter were quantified. In order to assess the effect of ERα, mTOR, and YAP signaling on CSC self-renewal capacity *in vitro*, tumor cells from untreated WT and mCol1a1 animals were treated with vehicle (0.1% ethanol, 0.1% DMSO, or both), 1 μM ICI, 10 nM rapamycin (Millipore Sigma, #553210), 1 μM verteporfin (Millipore Sigma, #SML0534), or combinations of inhibitors immediately after seeding into ultra-low attachment plates. After 10 days, primary tumorspheres were counted, dissociated with trypsin, and replated at 25,000 cells/well in mammosphere medium without treatments for an additional 10 days (secondary tumorsphere assay). Self-renewal was quantified by counting secondary tumorspheres.

2.5 Quantitative real-time PCR

Transcripts in single-cell tumor suspensions were quantified by qRT-PCR [25], normalized to 18S RNA. Primers with the following sequences were employed: *18S*: F: 5′-CGC CGC TAG AGG TGA AAT TCT-3′, R: 5′-CGA ACC TCC GAC TTT CGT TCT-3′; *Sox2*: F: 5′-CCA CCA ATC CCA TCC AAA TT-3′, R: 5′-CAA AAA GAA GTC CCA AGA TCT CTC A-3′; *Bmi1*: F: 5′-AGT TCG GCC AAC TTG CAA AA-3′, R: 5′-GCC TTG TCA CTC CCA GAG TC-3′; *Ctgf*: F: 5′-GTG TGC ACT GCC AAA GAT GG-3′, R: 5′-TGC TTT GGA AGG ACT CAC CG-3′; *Cyr61*: F: 5′-CAG CTC ACT GAA GAG GCT TCC T-3′, R: 5′-GCG TGC AGA GGG TTG AAA A-3′.

2.6 Immunoblotting

Protein lysates were prepared from single tumor cell suspensions, fractionated and immunoblotted for proteins of interest. Primary and secondary antibodies: AKT (1/2000; Cell Signaling Technologies, #9272), pAKT^{S473} (1/1000; Cell Signaling Technologies, #9271), p70S6k (1/1000; Cell Signaling Technologies, #9202), pp70S6k (1/1000; Cell Signaling Technologies, #9205), and HRP-linked anti-rabbit IgG (1/2000; Cell Signaling Technologies, #7074). Signals were visualized using enhanced chemiluminescence and quantified by scanning densitometry (Vision WorksLS, v7.1, UVP).

2.7 Statistical analysis

Data were analyzed using Prism v.5 (GraphPad Software, Inc., San Diego, CA). Based on our published studies which include quantification of some of these same endpoints [20,23], a sample size of 4 mice per group provides 95% power to detect a 30% difference with a 0.05 two-sided significance level. Experiments involving two groups were analyzed with Student's t-tests assuming unequal variance. For multiple experimental cohorts, data were analyzed by one-way ANOVA and multiple comparison tests. Differences were considered significant when $p<0.05$.

3. Results

3.1 Mammary tumors in mCol1a1 mice display abundant collagen deposition around tumor boundaries and generate increased lung metastases

To elucidate the effects of a desmoplastic collagen environment on the behavior of ERα+ tumors *in vivo*, tumor cells from a serially *in vivo* passaged prolactin-induced adenocarcinoma were orthotopically transplanted to mammary glands of WT and mCol1a1 young adult females. The resulting tumors exhibited similar histology, levels of ERα expression (Fig. 1Ai–iv), and rates of development in both recipient genotypes (Fig. 1B). However, tumors in the mCol1a1 hosts were surrounded by a dense collagenous network which was absent in WT hosts (Fig. 1Ai vs Aii).

To characterize the collagen matrix that enveloped these tumors, we stained tissues with picrosirius red (Fig. 1Av–viii). Collagen fibers around tumors in mCol1a1 hosts were more numerous (Fig. 1C) and more perpendicular to the tumor boundary (Fig. 1Aviii, arrows, Fig. 1D) compared to those in WT hosts. These characteristics resemble the tumor associated collagen signature-3 (TACS-3) [5], which in clinical cases, positively associates with tumor

grade and risk of metastasis, and predicts a decreased 10-year survival in ERα+ patients [4]. These results confirm that mCol1a1 mice model the desmoplasia which surrounds many cancers, and demonstrate that developing tumors in this environment interact with the ECM to realign collagen fibers, a feature associated with tumor progression.

To assess the impact of a dense collagen microenvironment on metastasis, we analyzed the lungs of tumor-burdened mice at end stage. Lungs of both WT and mCol1a1 recipients exhibited lesions, many of which contained ERα+ cells (Fig. 1E). However, metastases in mCol1a1 mice were significantly more numerous and larger (Fig. 1F,G) than in WT animals, suggesting that the desmoplastic ECM surrounding the tumors in mCol1a1 mice facilitates tumor cell invasion and intravasation, supported by other studies [6, 7, 23, 31].

3.2 Cancer stem cell activity and AKT-mTOR and YAP activities are increased in tumors in mCol1a1 mice

The impact of collagen properties on the CSC niche is of growing interest [32–34]. We therefore examined the effects of the desmoplastic microenvironment *in vivo* on CSC activity using the *in vitro* tumorsphere assay, an established method for studying stem-like activity [29, 30]. Mammary tumors from mCol1a1 hosts contained a significantly higher frequency of tumorsphere forming cells compared to tumors from WT hosts (Fig. 2A). Moreover, these tumors contained higher levels of transcripts for *Bmi1* and *Sox2*, which are associated with stem cell activity [35] (Fig. 2B), supporting the higher CSC frequency.

These findings led us to investigate signaling pathways which may link properties of the ECM to CSC activity, and may represent potential therapeutic targets. The PI3K-AKT-mTOR pathway has been linked to breast CSC self-renewal [13–15]. Activation of phosphoinositide 3-kinase (PI3K) phosphorylates AKT, which in turn, mediates formation of the mTOR complex 1 (mTORC1). Mammary tumors mCol1a1 recipients had significantly more phosphorylated AKT (pAKT) than WT tumors (Fig. 2C,D), and higher although more variable levels of phosphorylated p70S6K (pp70S6K), a downstream effector of mTOR (Fig. 2E). The Hippo transducer, YAP, which is activated by a dense/stiff ECM, also has been associated with increased CSC activity [10]. As predicted, tumors in mCol1a1 hosts exhibited nearly 3-fold more nuclear localized YAP (Fig. 2F,G), indicating higher activation. Consistently, they also contained elevated *Ctgf* and *Cyr61* mRNAs, target genes of this pathway (Fig. 2H) [36].

3.3 Inhibition of mTOR signaling reduces tumor volume and CSC activity

Many prolactin-induced ERα+ mammary tumors are no longer dependent on estrogen for growth [20], modeling advanced clinical anti-estrogen resistant cancers. The elevated CSC activity and activated signaling cascades implicated in CSCs, including pAKT and pp70S6K, in the mCol1a1 hosts suggested that mTOR inhibitors, approved therapies for ERα+ breast cancer [16–18], may counter the aggressive behaviors exhibited in a desmoplastic environment.

We therefore evaluated the mTOR inhibitor, rapamycin, and the SERD, ICI, to assess effects of mTOR inhibition in the context of the anti-estrogen treatment that patients with advanced ERα+ disease would receive. In one cohort, we initiated treatment of WT or mCol1a1 hosts

when the mammary tumors reached 150 mm^3, and continued the treatment for 14 days, when untreated control tumors had grown to end-stage size. As expected, ICI alone did not alter tumor growth in WT hosts [20] or mCol1a1 recipients (Fig. 3A). In contrast, rapamycin, alone or in combination with ICI, dramatically reduced mammary tumors to nearly undetectable volumes by 14 days in both WT and mCol1a1 animals (Fig. 3A, B), accompanied by widespread necrosis (Fig. S1B). In a second cohort, mice were treated for 14 days as described above, but then rapamycin/ICI treatment was withdrawn. Tumors quickly recovered in both WT and mCol1a1 mice, re-establishing pre-treatment volumes and collagen environments after an additional 14 days (Fig. 3B, Fig. S1B,C). These data demonstrate that these rapidly growing ERα+ mammary tumors are strongly dependent on mTOR signaling, regardless of host genotype, but that the therapeutic effect is not durable.

In light of the rapid recovery following treatment withdrawal, we evaluated the effect of treatment on CSC activity using the tumorsphere assay. Rapamycin, either alone or with ICI co-treatment, dramatically reduced CSC frequency in tumors from both host genotypes (Fig. 3C), demonstrating the crucial role of mTOR in this activity and its requirement for the increased CSC activity in the dense/stiff tumor microenvironment. After withdrawal of treatment, CSC activity increased in tumors from both genotypes, albeit to a lesser extent than tumor volume, reinforcing the importance of mTOR signals in CSC activity and the transient response to its inhibition. CSC activity in tumors from mCol1a1 recipients recovered significantly more rapidly after treatment withdrawal, confirming the enhanced CSC niche in mCol1a1 hosts.

To determine if treatment effects on CSC activity were independent of ongoing signals from the tumor microenvironment, we further examined the effects of ICI, rapamycin, and the YAP inhibitor, verteporfin, on CSC self-renewal *in vitro.* These compounds, alone or in combination, did not alter the frequency of primary tumorspheres that developed from cells harvested from untreated mammary tumors from either genotype, indicating that these inhibitors do not affect sphere-forming capacities of existing CSCs (Fig. S2). However, similar to previous findings, ICI treatment during formation of primary spheres, followed by dissociation and subsequent replating, increased development of secondary spheres in tumor cells from both host genotypes (Fig. 3D), indicating that ICI enhances CSC renewal [20, 37, 38]. In contrast, inhibition of either mTOR or YAP significantly decreased CSC self-renewal, regardless of host genotype, even in this *in vitro* setting (Fig. 3D). Moreover, inhibition of mTOR and YAP together was not additive (Fig. 3D), suggesting that their influence on CSC activity may be driven by a common signal in the mTOR pathway.

Together, these results confirm the individual importance of mTOR and YAP on tumor growth and CSC activity in these rapidly growing ERα+ but estrogen independent tumors, and strengthen our findings that desmoplastic tumor microenvironments enhance activation of both pathways.

3.4 Lung metastases are not dependent on mTOR signaling

In sharp contrast to the mTOR dependent growth and CSC activity of the mammary tumors, lung metastases in both WT and mCol1a1 hosts were strikingly unresponsive to rapamycin/ICI co-treatment (Fig. 4A–C, compare to Fig. 1E–G), leaving mCol1a1 recipients

with more abundant and larger lung lesions. Whereas mammary tumors displayed elevated cleaved caspase-3 expression two days after initiation of treatment, preceding extensive necrosis evident after 14 days (Fig. S1B), the corresponding lung metastases displayed low apoptosis even after 14 days of treatment (Fig. 4D, Fig. S3A). Examination of pS6RP staining in mammary tumors and pulmonary lesions of untreated animals revealed significantly lower mTOR activity in the metastases, consistent with differential dependence of local and metastatic lesions on mTOR (Fig. 4E, Fig. S3B). Furthermore, in untreated animals, lung lesions were significantly less proliferative than mammary tumors (Fig. 4F–G). These results suggest that the pulmonary environment fosters lesions with less mTOR activity and consequent resistance to mTOR inhibitors by selecting for escaped tumor cells with these features and/or supporting lower rates of growth [39–41].

4. Discussion

Treatment resistance occurs in more than a quarter of all patients with ERα+ breast cancer, and many of these individuals eventually succumb to metastatic disease. The mechanisms underlying treatment failure are unclear, but several features, including CSCs and a surrounding dense/stiff ECM, have been implicated in tumor aggression and therapy resistance. Studies have been limited by the paucity of preclinical *in vivo* models. Using a serially transplantable heterogeneous prolactin-induced ERα+ adenocarcinoma to model anti-estrogen resistant clinical cancers, we demonstrated that the desmoplastic environment which develops rapidly around mammary tumors in mCol1a1 recipients increases CSC activity without altering tumor growth, and augments the number and size of lung metastases. This was associated with increased AKT-mTOR and YAP activity in mammary tumors in the mCol1a1 environment, suggesting that the heightened aggression could be ameliorated by mTOR inhibitors, which are approved for treatment of advanced ERα+ cancers. However, although rapamycin dramatically reduced mammary tumor cell survival and CSC activity, this effect was not durable. Moreover, lung metastases were strikingly resistant, and mCol1a1 recipients continued to bear a greater metastatic burden.

A burgeoning literature documents the growing interest in YAP/TAZ signals in cancer. Our *in vivo* studies of metastatic ERα+ cancer substantiate the links established in elegant *in vitro* studies between stiff ECMs and YAP/TAZ activation (reviewed in [10, 36, 42]) and ECM stiffness and CSC activity in breast cancer cells [33], and TAZ and CSC activity in mouse models and clinical cancers (reviewed in [10]). Our examination of CSC activity *in vitro* also reveals a connection between YAP and the PI3K-AKT-mTOR pathway, demonstrated in tissue growth and hyperplasia [43]. Together, our data support the model that desmoplastic collagen microenvironments activate AKT-mTOR signaling and thereby enhance CSC activity in ERα+ cancers. mTOR-targeted therapies have shown some promise in patients with anti-estrogen resistant ERα+ breast cancers [16–18]. Ongoing trials in various settings of breast cancer are demonstrating increases in progression-free-survival, although overall survival data are not yet mature. However, our findings also suggest that analysis of metastatic sites might be particularly informative.

Despite dramatic impacts on tumor cell survival and CSC activity of established mammary tumors, targeting mTOR failed to impact lung metastases. Although these metastases

displayed a more indolent phenotype than the aggressive parent tumors, their persistence in the face of treatment that dramatically reduced the mammary tumors suggests that these distant lesions may lead to symptomatic disease even after successful treatment of the primary tumor. Interestingly, Mateo and colleagues recently reported in a model of triple negative breast cancer that mTOR signaling was important for initiation of distant metastases, but also noted that many established metastatic lesions were resistant to mTOR inhibition [44]. Therefore differences in treatment sensitivity at primary and pulmonary sites are not restricted to a specific breast cancer subtype.

Epidemiologically, prolactin exposure is associated with higher risk for development of aggressive ERα+ breast cancer [45, 46]. Increased mammary exposure to prolactin as modeled in the transgenic NRL-PRL mouse results in spontaneous diverse mammary carcinomas, many of which express ERα. The serially *in vivo* passaged heterogeneous adenocarcinomas that have not been exposed to tissue culture plastic, such as that employed here, exhibit diverse morphologies and behaviors [20]. Together with cell lines derived from these tumors [23, 47], they provide preclinical models of ERα+ breast cancer to examine disease processes in the dynamic immunocompetent *in vivo* environment.

In summary, our findings demonstrate the ability of desmoplastic ECMs *in vivo* to enhance CSC activity in mammary ERα+ tumors by both mTOR and YAP signals, associated with increased pulmonary metastases. The resistance of lung lesions to mTOR inhibitors, in contrast to the primary tumors, underscores the different therapeutic responses of local tumors and distant lesions; a complete pathologic response at the primary site may not translate to successful treatment of distant metastases. Analysis of long term outcomes in ongoing patient trials and future experimental studies are needed to illuminate susceptibility/resistance to inhibitors of mTOR and related pathways at different metastatic sites.

Supplementary Material

Refer to Web version on PubMed Central for supplementary material.

Acknowledgments

The authors thank Debra Rugowski for valuable assistance with immunohistochemical analyses, and Kevin Eliceiri and the UW Laboratory for Optical and Computational Instrumentation (LOCI) for help with collagen analysis.

Funding Sources

This work was supported by the National Institutes of Health [R01CA157675 and R01CA179556 (LAS), T32ES007015 (MPS, KAW), U54DK104310 (CMV), F31ESO28594 (KAW), P30CA014520 (University of Wisconsin Carbone Cancer Center)]. Its contents are solely the responsibility of the authors and do not necessarily represent the official views of the NIEHS, NIH.

References

1. Ades F, Zardavas D, Bozovic-Spasojevic I, Pugliano L, Fumagalli D, de Azambuja E, Viale G, Sotiriou C, Piccart M. Luminal B breast cancer: Molecular characterization, clinical management, and future perspectives. J Clin Oncol. 2014; 32:2794–2803. [PubMed: 25049332]
2. Davies C, Godwin J, Gray R, Clarke M, Cutter D, Darby S, McGale P, Pan HC, Taylor C, Wang YC, Dowsett M, Ingle J, Peto R. G. Early Breast Cancer Trialists' Collaborative. Relevance of breast

cancer hormone receptors and other factors to the efficacy of adjuvant tamoxifen: Patient-level meta-analysis of randomised trials. Lancet. 2011; 378:771–784. [PubMed: 21802721]

3. Vachon CM, van Gils CH, Sellers TA, Ghosh K, Pruthi S, Brandt KR, Pankratz VS. Mammographic density, breast cancer risk and risk prediction. Breast Cancer Res. 2007; 9:217. [PubMed: 18190724]
4. Conklin MW, Eickhoff JC, Riching KM, Pehlke CA, Eliceiri KW, Provenzano PP, Friedl A, Keely PJ. Aligned collagen is a prognostic signature for survival in human breast carcinoma. The Am J Pathol. 2011; 178:1221–1232. [PubMed: 21356373]
5. Provenzano PP, Eliceiri KW, Campbell JM, Inman DR, White JG, Keely PJ. Collagen reorganization at the tumor-stromal interface facilitates local invasion. BMC Med. 2006; 4:38. [PubMed: 17190588]
6. Schedin P, Keely PJ. Mammary gland ECM remodeling, stiffness, and mechanosignaling in normal development and tumor progression. Cold Spring Harbor Perspect Biol. 2011; 3:a003228.
7. Pickup MW, Mouw JK, Weaver VM. The extracellular matrix modulates the hallmarks of cancer. EMBO Reports. 2014; 15:1243–1253. [PubMed: 25381661]
8. Easwaran H, Tsai HC, Baylin SB. Cancer epigenetics: Tumor heterogeneity, plasticity of stem-like states, and drug resistance. Mol Cell. 2014; 54:716–727. [PubMed: 24905005]
9. Wei W, Lewis MT. Identifying and targeting tumor-initiating cells in the treatment of breast cancer. Endocr Relat Cancer. 2015; 22:R135–155. [PubMed: 25876646]
10. Zanconato F, Cordenonsi M, Piccolo S. Yap/Taz at the roots of cancer. Cancer Cell. 2016; 29:783–803. [PubMed: 27300434]
11. Al Hajj M, Wicha MS, Benito-Hernandez A, Morrison SJ, Clarke MF. Prospective identification of tumorigenic breast cancer cells. Proc Natl Acad Sci USA. 2003; 100:3983–3988. [PubMed: 12629218]
12. Nassar D, Blanpain C. Cancer stem cells: Basic concepts and therapeutic implications. Ann Rev Pathol. 2016; 11:47–76. [PubMed: 27193450]
13. Xia P, Xu XY. Pi3k/akt/mtor signaling pathway in cancer stem cells: From basic research to clinical application. Am J Can Res. 2015; 5:1602–1609.
14. Martelli AM, Evangelisti C, Follo MY, Ramazzotti G, Fini M, Giardino R, Manzoli L, McCubrey JA, Cocco L. Targeting the phosphatidylinositol 3-kinase/AKT/mammalian target of rapamycin signaling network in cancer stem cells. Curr Med Chem. 2011; 18:2715–2726. [PubMed: 21649579]
15. Zhou J, Wulfkuhle J, Zhang H, Gu P, Yang Y, Deng J, Margolick JB, Liotta LA, Petricoin E 3rd, Zhang Y. Activation of the pten/mtor/stat3 pathway in breast cancer stem-like cells is required for viability and maintenance. Proc Natl Acad Sci U S A. 2007; 104:16158–16163. [PubMed: 17911267]
16. Paplomata E, O'Regan R. The pi3k/akt/mtor pathway in breast cancer: Targets, trials and biomarkers. Ther Adv Med Oncol. 2014; 6:154–166. [PubMed: 25057302]
17. Yi Z, Ma F. Biomarkers of everolimus sensitivity in hormone receptor-positive breast cancer. J Br Cancer. 2017; 20:321–326.
18. Royce ME, Osman D. Everolimus in the treatment of metastatic breast cancer. Breast cancer: Basic Clin Res. 2015; 9:73–79.
19. O'Leary KA, Shea MP, Schuler LA. Modeling prolactin actions in breast cancer in vivo: Insights from the NRL-PRL mouse. Adv Exp Med Biol. 2015; 846:201–220. [PubMed: 25472540]
20. Shea MP, O'Leary KA, Fakhraldeen SA, Goffin V, Friedl A, Wisinski KB, Alexander CM, Schuler LA. Anti-estrogen therapy increases plasticity and cancer stemness of prolactin-induced ERα+ mammary carcinomas. Cancer Res. 2018:1672–1684. [PubMed: 29363543]
21. Liu X, Wu H, Byrne M, Jeffrey J, Krane S, Jaenisch R. A targeted mutation at the known collagenase cleavage site in mouse type I collagen impairs tissue remodeling. J Cell Biol. 1995; 130:227–237. [PubMed: 7790374]
22. Provenzano PP, Inman DR, Eliceiri KW, Knittel JG, Yan L, Rueden CT, White JG, Keely PJ. Collagen density promotes mammary tumor initiation and progression. BMC Med. 2008; 6:11. [PubMed: 18442412]

23. Barcus CE, O'Leary KA, Brockman JL, Rugowski DE, Liu Y, Garcia N, Yu M, Keely PJ, Eliceiri KW, Schuler LA. Elevated collagen-I augments tumor progressive signals, intravasation and metastasis of prolactin-induced estrogen receptor alpha positive mammary tumor cells. Breast Cancer Res. 2017; 19:9. [PubMed: 28103936]
24. Rose-Hellekant TA, Arendt LM, Schroeder MD, Gilchrist K, Sandgren EP, Schuler LA. Prolactin induces ERα-positive and ERα-negative mammary cancer in transgenic mice. Oncogene. 2003; 22:4664–4674. [PubMed: 12879011]
25. Arendt LM, Rugowski DE, Grafwallner-Huseth TL, Garcia-Barchino MJ, Rui H, Schuler LA. Prolactin-induced mouse mammary carcinomas model estrogen resistant luminal breast cancer. Breast Cancer Res. 2011; 13:R11–25. [PubMed: 21276249]
26. Schneider CA, Rasband WS, Eliceiri KW. NIH image to ImageJ: 25 years of image analysis. Nature Meth. 2012; 9:671–675.
27. Wegner KA, Keikhosravi A, Eliceiri KW, Vezina CM. Fluorescence of picrosirius red multiplexed with immunohistochemistry for the quantitative assessment of collagen in tissue sections. J Histochem Cytochem. 2017; 65:479–490. [PubMed: 28692327]
28. Liu Y, Keikhosravi A, Mehta GS, Drifka CR, Eliceiri KW. Methods for quantifying fibrillar collagen alignment. Methods Mol Biol. 2017; 1627:429–451. [PubMed: 28836218]
29. Kim S, Alexander CM. Tumorsphere assay provides more accurate prediction of in vivo responses to chemotherapeutics. Biotechnol Lett. 2014; 36:481–488. [PubMed: 24158677]
30. Shaw FL, Harrison H, Spence K, Ablett MP, Simoes BM, Farnie G, Clarke RB. A detailed mammosphere assay protocol for the quantification of breast stem cell activity. J Mammary Gland Biol Neoplasia. 2012; 17:111–117. [PubMed: 22665270]
31. Clark AG, Vignjevic DM. Modes of cancer cell invasion and the role of the microenvironment. Curr Opin Cell Biol. 2015; 36:13–22. [PubMed: 26183445]
32. Plaks V, Kong N, Werb Z. The cancer stem cell niche: How essential is the niche in regulating stemness of tumor cells? Cell Stem Cell. 2015; 16:225–238. [PubMed: 25748930]
33. Pang MF, Siedlik MJ, Han S, Stallings-Mann M, Radisky DC, Nelson CM. Tissue stiffness and hypoxia modulate the integrin-linked kinase ILK to control breast cancer stem-like cells. Cancer Res. 2016; 76:5277–5287. [PubMed: 27503933]
34. Vining KH, Mooney DJ. Mechanical forces direct stem cell behaviour in development and regeneration. Nature Rev Mol Cell Biol. 2017; 18:728–742. [PubMed: 29115301]
35. Hadjimichael C, Chanoumidou K, Papadopoulou N, Arampatzi P, Papamatheakis J, Kretsovali A. Common stemness regulators of embryonic and cancer stem cells. World J Stem Cells. 2015; 7:1150–1184. [PubMed: 26516408]
36. Dupont S. Role of Yap/Taz in cell-matrix adhesion-mediated signalling and mechanotransduction. Exp Cell Res. 2016; 343:42–53. [PubMed: 26524510]
37. Simoes BM, O'Brien CS, Eyre R, Silva A, Yu L, Sarmiento-Castro A, Alferez DG, Spence K, Santiago-Gomez A, Chemi F, Acar A, Gandhi A, Howell A, Brennan K, Ryden L, Catalano S, Ando S, Gee J, Ucar A, Sims AH, Marangoni E, Farnie G, Landberg G, Howell SJ, Clarke RB. Anti-estrogen resistance in human breast tumors is driven by JAG1-NOTCH4-dependent cancer stem cell activity. Cell Reports. 2015; 12:1968–1977. [PubMed: 26387946]
38. Karthik GM, Ma R, Lovrot J, Kis LL, Lindh C, Blomquist L, Fredriksson I, Bergh J, Hartman J. mTOR inhibitors counteract tamoxifen-induced activation of breast cancer stem cells. Cancer Lett. 2015; 367:76–87. [PubMed: 26208432]
39. Obenauf AC, Zou Y, Ji AL, Vanharanta S, Shu W, Shi H, Kong X, Bosenberg MC, Wiesner T, Rosen N, Lo RS, Massague J. Therapy-induced tumour secretomes promote resistance and tumour progression. Nature. 2015; 520:368–372. [PubMed: 25807485]
40. Yeh AC, Ramaswamy S. Mechanisms of cancer cell dormancy--another hallmark of cancer? Cancer Res. 2015; 75:5014–5022. [PubMed: 26354021]
41. Lambert AW, Pattabiraman DR, Weinberg RA. Emerging biological principles of metastasis. Cell. 2017; 168:670–691. [PubMed: 28187288]
42. Moroishi T, Hansen CG, Guan KL. The emerging roles of Yap and Taz in cancer. Nat Rev Cancer. 2015; 15:73–79. [PubMed: 25592648]

43. Tumaneng K, Schlegelmilch K, Russell RC, Yimlamai D, Basnet H, Mahadevan N, Fitamant J, Bardeesy N, Camargo FD, Guan KL. Yap mediates crosstalk between the Hippo and PI(3)K-TOR pathways by suppressing PTEN via mir-29. Nat Cell Biol. 2012; 14:1322–1329. [PubMed: 23143395]

44. Mateo F, Arenas EJ, Aguilar H, Serra-Musach J, de Garibay GR, Boni J, Maicas M, Du S, Iorio F, Herranz-Ors C, Islam A, Prado X, Llorente A, Petit A, Vidal A, Catala I, Soler T, Venturas G, Rojo-Sebastian A, Serra H, Cuadras D, Blanco I, Lozano J, Canals F, Sieuwerts AM, de Weerd V, Look MP, Puertas S, Garcia N, Perkins AS, Bonifaci N, Skowron M, Gomez-Baldo L, Hernandez V, Martinez-Aranda A, Martinez-Iniesta M, Serrat X, Ceron J, Brunet J, Barretina MP, Gil M, Falo C, Fernandez A, Morilla I, Pernas S, Pla MJ, Andreu X, Segui MA, Ballester R, Castella E, Nellist M, Morales S, Valls J, Velasco A, Matias-Guiu X, Figueras A, Sanchez-Mut JV, Sanchez-Cespedes M, Cordero A, Gomez-Miragaya J, Palomero L, Gomez A, Gajewski TF, Cohen EEW, Jesiotr M, Bodnar L, Quintela-Fandino M, Lopez-Bigas N, Valdes-Mas R, Puente XS, Vinals F, Casanovas O, Graupera M, Hernandez-Losa J, Ramon YCS, Garcia-Alonso L, Saez-Rodriguez J, Esteller M, Sierra A, Martin-Martin N, Matheu A, Carracedo A, Gonzalez-Suarez E, Nanjundan M, Cortes J, Lazaro C, Odero MD, Martens JWM, Moreno-Bueno G, Barcellos-Hoff MH, Villanueva A, Gomis RR, Pujana MA. Stem cell-like transcriptional reprogramming mediates metastatic resistance to mTOR inhibition. Oncogene. 2017; 36:2737–2749. [PubMed: 27991928]

45. Tworoger SS, Eliassen AH, Zhang X, Qian J, Sluss PM, Rosner BA, Hankinson SE. A 20-year prospective study of plasma prolactin as a risk marker of breast cancer development. Cancer Res. 2013; 73:4810–4819. [PubMed: 23783576]

46. Tikk K, Sookthai D, Johnson T, Rinaldi S, Romieu I, Tjonneland A, Olsen A, Overvad K, Clavel-Chapelon F, Baglietto L, Boeing H, Trichopoulou A, Lagiou P, Trichopoulos D, Palli D, Pala V, Tumino R, Rosso S, Panico S, Agudo A, Menendez V, Sanchez MJ, Amiano P, Huerta Castano JM, Ardanaz E, Bueno-de-Mesquita HB, Monninkhof E, Onland-Moret C, Andersson A, Sund M, Weiderpass E, Khaw KT, Key TJ, Travis RC, Gunter MJ, Riboli E, Dossus L, Kaaks R. Circulating prolactin and breast cancer risk among pre- and postmenopausal women in the epic cohort. Ann Oncol. 2014; 25:1422–1428. [PubMed: 24718887]

47. Jallow F, Brockman JL, Helzer KT, Rugowski DE, Goffin V, Alarid ET, Schuler LA. 17β-estradiol and ICI182,780 differentially regulate Stat5 isoforms in female mammary epithelium, with distinct outcomes. J Endocr Soc. 2018; 2:293–309. [PubMed: 29594259]

Highlights

- Dense/stiff microenvironments enhanced CSC activity, AKT-mTOR and YAP activation
- Inhibition of mTOR +/− ICI182780 rapidly but not durably diminished mammary tumors
- Lung metastases, which exhibited lower mTOR activity, were unresponsive
- mCol1a1 hosts continued to sustain greater metastatic burdens despite treatment

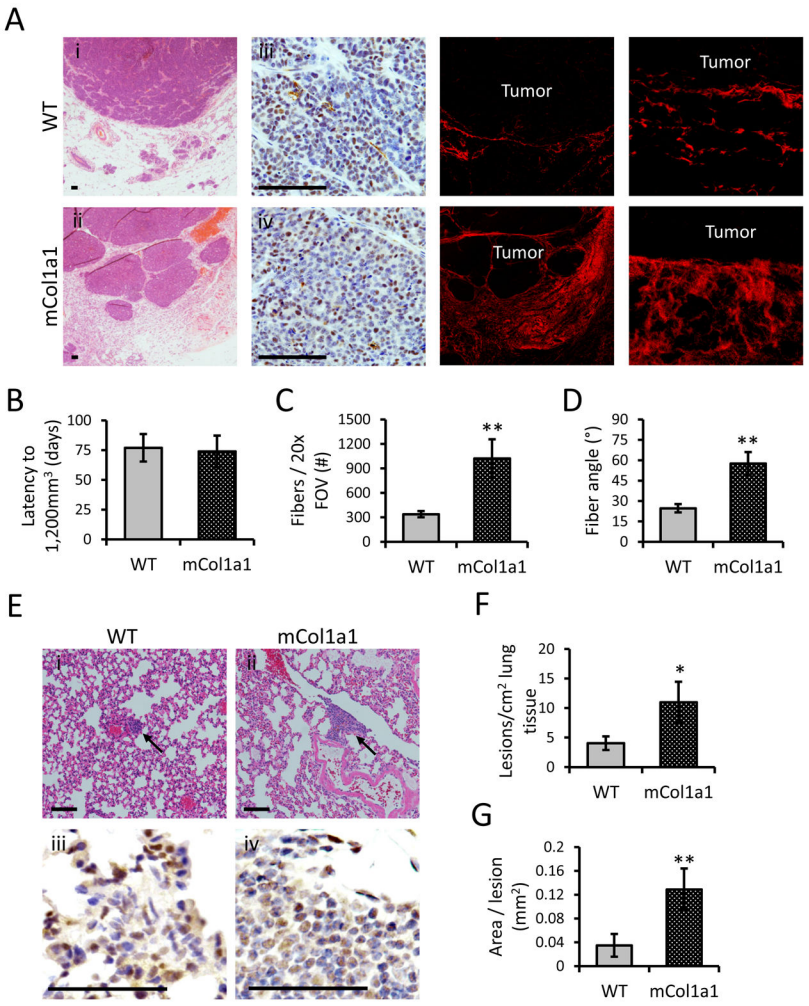

Figure 1. mCol1a1 recipients display increased deposition of fibrillar collagen around primary tumors and higher metastatic load

100,000 tumor cells from a serially passaged ERα+ NRL-PRL adenocarcinoma were transplanted into mammary fat pads of either WT or mCol1a1 mice, and growth of the primary tumor was monitored until end stage. (A) i,ii; Representative H&E stained photomicrographs of end-stage tumors and the adjacent mammary gland in WT and mCol1a1 mice. Scale bars, 100 μm. iii,iv; ERα expression, representative images. Scale bars, 100 μm. v-viii; Picrosirius red-stained collagen, visualized by fluorescent confocal microscopy. Scale bars, 100 μm. (B) Tumor latency (days) from initial transplantation until tumors grew to approximate end-stage volume, 1,200 mm^3 (N=4 tumors; mean ± S.D.). (C) Quantification of collagen fibers using CT-FIRE analysis, see Methods (N=4 tumors; mean ± S.D.). (D) Collagen fiber alignment angle relative to the tumor boundaries using CurveAlign analysis, see Methods. * $p<0.05$, ** $p<0.01$ by unpaired Student's t-tests. (E) Lung metastases in WT and mCol1a1 mice. i,ii: H&E; iii,iv: ERα. Scale bars, 100 μm. (F) Numbers of lung metastases per cm^2 lung tissue, quantified as described in the Materials and Methods (N=4 animals; mean ± S.D.). (G) Average lung lesion area (N=4 animals; mean ± S.D.). * $p<0.05$, ** $p<0.01$ by unpaired Student's t-tests.

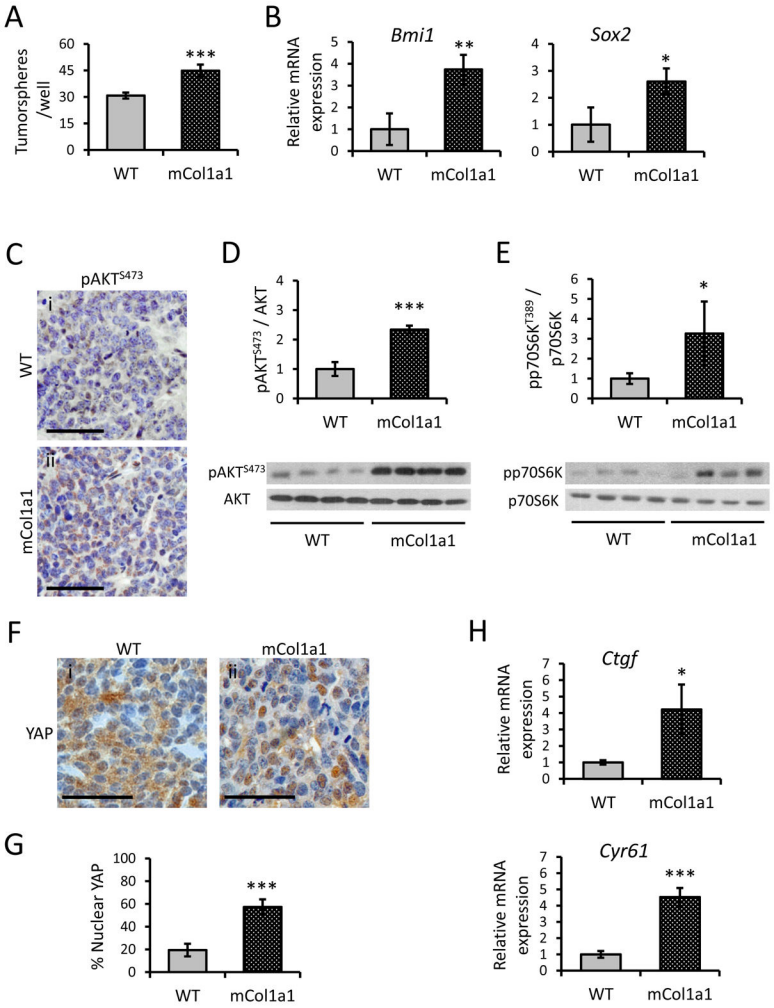

Figure 2. Tumors from mCol1a1 hosts display elevated CSC activity and associated signaling pathways

(A) Ability of tumor cells in WT and mCol1a1 recipients to form primary tumorspheres (N=4 tumors; mean ± S.D.). (B) Relative transcript levels of *Bmi1* and *Sox2* in tumors from WT and mCol1a1 recipients as measured by qRT-PCR (N=4 tumors; mean ± S.D.). (C) pAKT^{S473} immunostaining of primary tumors (representative images). Scale bars, 50 μm. (D) Immunoblotting of pAKT^{S473} relative to total AKT protein (N=4 tumors; mean ± S.D.). (E) Immunoblotting of pp70S6k^{T389} relative to total p70S6K protein (N=4 tumors; mean ± S.D.). (F) YAP immunostaining of primary tumors (representative images). Scale bars, 50 μm. (G) Quantification of YAP nuclear localization (N=4 independent tumors; mean ± S.D.). (H) Relative transcripts of YAP target genes, *Ctgf* and *Cyr61* (N=4 tumors; mean ± S.D.). * p<0.05, ** p<0.01, *** p<0.001 by unpaired Student's t-tests.

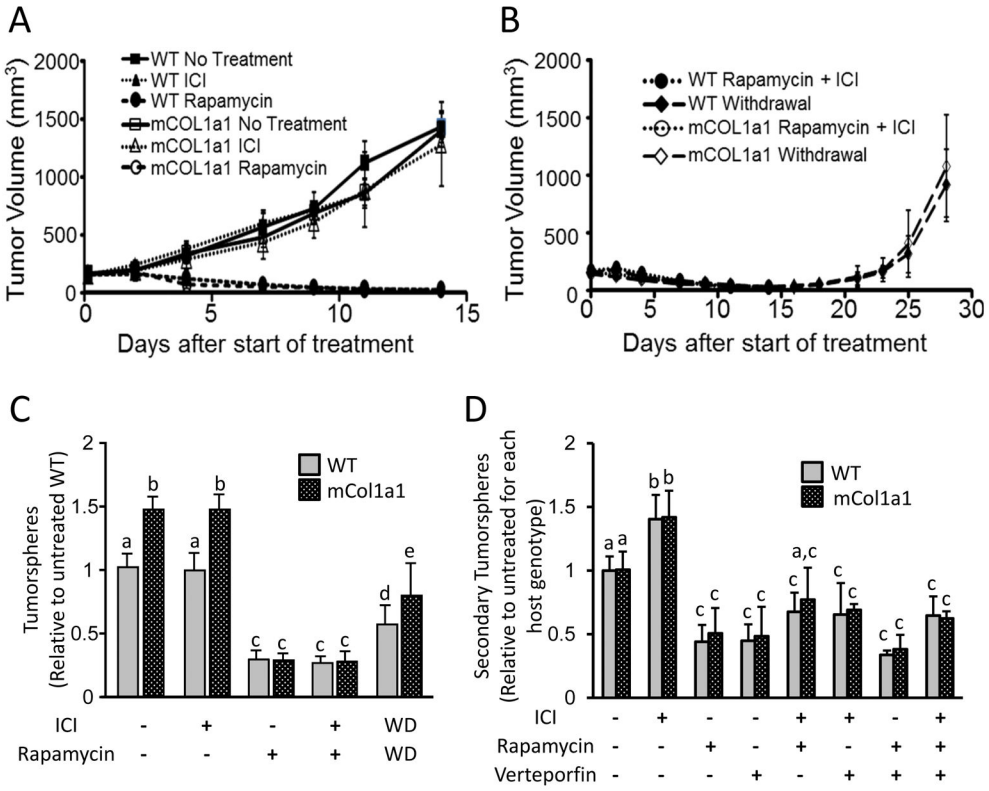

Figure 3. Rapamycin diminishes tumor volume and CSC activity, regardless of host environment

(A,B) Effect of treatment on the volume of primary tumors after initiation and withdrawal of treatment for an additional 14 days as shown (N=4 tumors per treatment group; mean ± S.D.). (C) Effects of *in vivo* treatments on ability to form primary tumorspheres *in vitro* (N=4 tumors; mean ± S.D.). (D) Effects of *in vitro* treatments on CSC self-renewal, as assessed by secondary tumorsphere formation. Data are normalized to the number of tumorspheres that develop in untreated cells from tumors from each host genotype, respectively. (N=4 independent experiments; mean ± S.D.). C, D. Different letters denote significant differences among groups (one-way ANOVA followed by Tukey's multiple comparison tests, $p<0.05$).

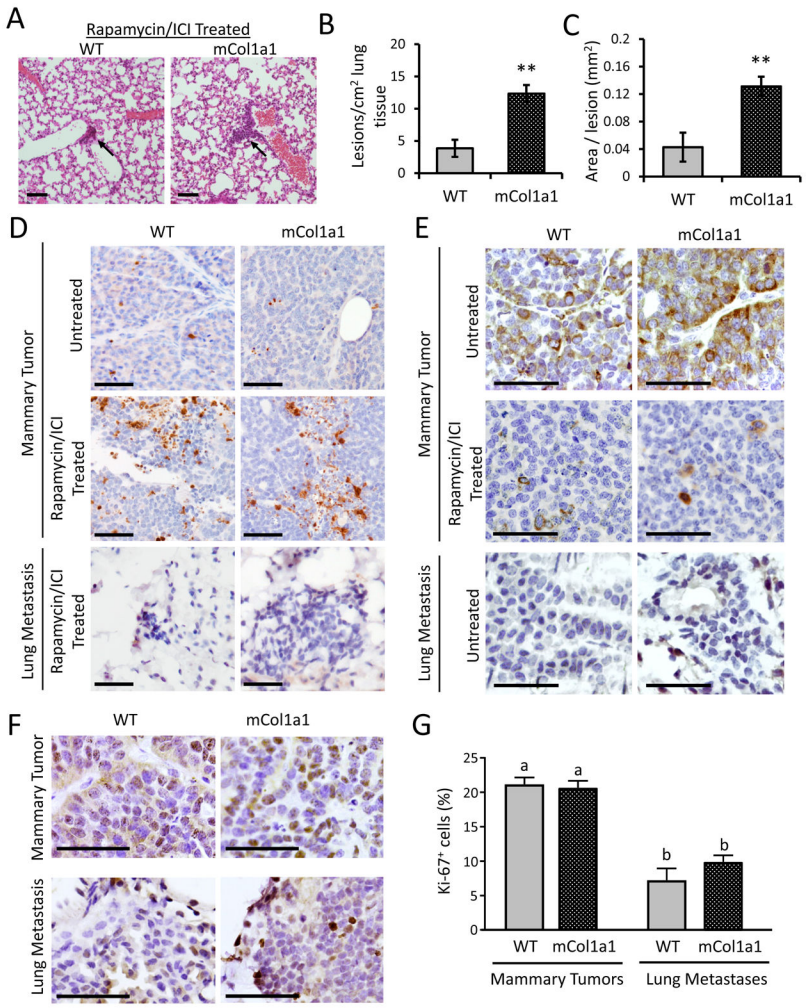

Figure 4. Lung metastases are unaffected by *in vivo* Rapamycin/ICI treatment

(A) Representative images of lung metastases in mice treated with Rapamycin/ICI for 14 days. Scale bars, 100 μm. (B) Number of lung lesions per cm^2 tissue. (C) Size of lung lesions. (N=4 mice; mean ± S.D.). ** $p<0.01$ by unpaired Student's t-test. (D) Apoptosis, indicated by immunohistochemical staining for cleaved caspase-3, in primary tumors from untreated hosts, primary tumors from hosts treated with Rapamycin/ICI for 2 days, and lung metastases from hosts treated with Rapamycin/ICI for 14 days. Scale bars, 100 μm. (Positive cells quantified in Supplementary Figure 3A). (E) $pS6RP^{S235/236}$ staining in primary tumors from untreated and ICI/Rapamycin-treated (2 day) hosts and lung metastases from untreated hosts. Scale bars, 100 μm. (Positive cells quantified in Supplementary Figure 3B). (F) Proliferation in primary tumors and lung metastases from untreated hosts, indicated by Ki-67 staining. Scale bars, 100 μm. (G) Quantification of Ki-67 positive cells from (F) (N= 4 mice; Mean ± S.D.). Different letters denote significant differences (one-way ANOVA followed by Tukey's multiple comparison tests), $p<0.05$.